

**Short Communication:****Design of Defect and Metallic Silver in Silver Phosphate Photocatalyst Using the Hydroxyapatite and Glucose**Uyi Sulaeman<sup>1,\*</sup>, Suhendar Suhendar<sup>1</sup>, Hartiwi Diastuti<sup>1</sup>, Roy Andreas<sup>1</sup>, and Shu Yin<sup>2</sup><sup>1</sup>Department of Chemistry, Universitas Jenderal Soedirman,  
Jl. dr. Soeparno 61, Karangwangkal, Purwokerto 53123, Indonesia<sup>2</sup>Institute of Multidisciplinary Research for Advanced Materials, Tohoku University, Sendai, 980-8577, Japan**\* Corresponding author:**

email: sulaeman@unsoed.ac.id

Received: August 10, 2019

Accepted: April 29, 2020

DOI: 10.22146/ijc.48647

**Abstract:** The defect and metallic silver (Ag) in silver phosphate ( $\text{Ag}_3\text{PO}_4$ ) photocatalyst were successfully generated using hydroxyapatite (HA) and glucose. Two steps of synthesis were done in these experiments. Firstly, the Ag/HA powder was prepared by reacting  $\text{AgNO}_3$  and HA, followed by the addition of a glucose solution. Secondly, the suspension of Ag/HA was reacted with  $\text{AgNO}_3$  aqueous solution. The yellow product of Ag/ $\text{Ag}_3\text{PO}_4$  photocatalyst was produced. The products were characterized using X-Ray Diffraction (XRD), Diffuse Reflectance Spectroscopy (DRS), Scanning Electron Microscope (SEM), Brunauer–Emmett–Teller (BET) and X-ray Photoelectron Spectroscopy (XPS). The decreased ratio of O/Ag and metallic Ag formation observed by the XPS was detected as the possible defect and Ag-doping in the photocatalyst. The enhanced photocatalytic activity might be caused by the oxygen vacancy and metallic Ag in  $\text{Ag}_3\text{PO}_4$  that enables the separation of photo-generated electrons and holes.

**Keywords:**  $\text{Ag}_3\text{PO}_4$ ; glucose; hydroxyapatite; oxygen vacancy

**■ INTRODUCTION**

Recently, metallic Ag-doping ( $\text{Ag}^0$ ) in photocatalyst has been widely developed to improve the ability of photocatalytic properties. The metallic Ag dopant could increase the photocatalytic activity of  $\text{Ag}_3\text{PO}_4$  through enhancing the separation of electrons and holes, and generating the plasmon surface resonance [1-2]. Formation of Ag at the early photocatalytic reaction in  $\text{Ag}_3\text{PO}_4/\text{Bi}_2\text{WO}_6$  showed an excellent photostability due to the role of Ag served as the bridge of charge transmission to prevent a further photoreduction of  $\text{Ag}_3\text{PO}_4$  [3]. The function of metallic Ag as a charge mediator was also found in CdSe and  $\text{Ag}_3\text{PO}_4$  [4]. The metallic Ag in g- $\text{C}_3\text{N}_4/\text{Ag}/\text{Ag}_3\text{PO}_4$  composite can act as the center of Z-mechanism to improve the photocatalytic activity [5]. The metallic Ag incorporated on the  $\text{Ag}_3\text{PO}_4$  can be prepared by using pyridine as a reducing agent [6], ammonia with glucose/ $\text{NaBH}_4$  [7], and photo-irradiation [8].

Besides the metallic Ag dopant, the defect generated in photocatalyst could dramatically enhance catalytic activity. Based on a previous result [9], the coprecipitation under mixed water-ethanol solution generates the silver vacancy defect. This defect significantly increases catalytic activity. The silver vacancies and  $\text{Ag}^0$  in  $\text{Ag}_3\text{PO}_4$  can also be treated by ammonia [10]. This preparation narrowed the bandgap energies that improves the photocatalytic activity of  $\text{Ag}_3\text{PO}_4$ . The surface defects in  $\text{Ag}_3\text{PO}_4$  could also be created by La doping [11]. The surface defects and porous surface formation in La- $\text{Ag}_3\text{PO}_4$  improves the photocatalytic activity. Amongst the defects, the oxygen vacancy is very promising to improve the photocatalytic reaction. It can be created under heat treatment [12-13]. Based on the reports, it is beneficial to generate the defect in  $\text{Ag}_3\text{PO}_4$  to improve the photocatalytic reaction.

The significant performance of  $\text{Ag}_3\text{PO}_4$  can also be prepared by hydroxyapatite (HA) as a substrate of

phosphate [14]. This preparation successfully decreases the particle size and increases the visible absorption. Therefore, to obtain highly active photocatalyst, the creation of metallic Ag on  $\text{Ag}_3\text{PO}_4$  using glucose and hydroxyapatite simultaneously, would be a novel and promising alternative to enhance activity. The task is very challenging because glucose and hydroxyapatite is an inexpensive and abundant material.

Herein, the defect and metallic Ag were easily generated in  $\text{Ag}_3\text{PO}_4$  using glucose as a reductant and HA as the substrate of phosphate ion. The type defect of oxygen vacancy was formed due to reducing  $\text{Ag}^+$  to metallic Ag. These phenomena improve the catalytic activity of  $\text{Ag}_3\text{PO}_4$ .

## ■ EXPERIMENTAL SECTION

### Materials

The starting material of  $\text{AgNO}_3$  was purchased from Merck. The  $\text{CaCl}_2$ ,  $\text{KH}_2\text{PO}_4$ , and ethylenediamine were purchased from Merck and used for hydroxyapatite synthesis. A reducing agent, glucose solution, was prepared using D(+)glucose anhydrous (Merck). Rhodamine B (RhB) was purchased from Merck and used for photocatalytic activity evaluation. All materials were of analytical reagent grade and used without further purification.

### Instrumentation

The XRD pattern of crystals was recorded using Shimadzu XRD-7000 at the range of  $10\text{--}80^\circ 2\theta$  ( $\text{CuK}\alpha = 1.54056 \text{ \AA}$ , 30 kV, 30 mA, step width  $0.02^\circ$ , and scan speed  $3.0^\circ/\text{min}$ ). Absorptions and bandgap energies were analyzed using UV-vis DRS (JASCO V-670). The specific surface areas and porosity were measured using BET (NOVA instruments). Morphology of crystals was observed by SEM (Jeol JSM 6510 LA). The core level, binding energy, and atomic ratio were analyzed using XPS (Perkin Elmer PHI 5600). To obtaining the accurate composition of  $\text{Ag}_3\text{PO}_4$ , the samples were treated by argon ( $\text{Ar}^+$ ) sputtering at 3 KeV for 2 min before the analysis.

The photocatalytic reaction was carried in the box reactor. A blue LED lamp (Duralux, 3 Watt) was used as a source of irradiation that was placed at 10 cm above the

solution. The decreased RhB concentration was monitored using a UV-vis spectrophotometer (Shimadzu UV-1800).

### Procedure

#### Synthesis of Ag/HA precursor

The Ag/HA precursor was synthesized using the  $\text{AgNO}_3$  and HA. The HA was synthesized based on a method by Wang et al. with modification [15]. A 100 mL of 1 M  $\text{CaCl}_2$  solution was added slowly dropwise into a 100 mL of 0.6 M  $\text{KH}_2\text{PO}_4$  solution under pH 8, adjusted by ethylenediamine. The product was filtered and dried in an oven at  $60^\circ\text{C}$  for 2 h. An amount of 0.5 g of HA was suspended in 100 mL of water and added to a 3.6 mL of 0.1 M  $\text{AgNO}_3$  (0.36 mmol). The suspensions were stirred for 20 min and sonicated at room temperature for 5 min. The suspensions were added into 14.4 mL of 0.1 M glucose solution (mole ratio of glucose/ $\text{AgNO}_3 = 4$ ), mixed at  $80^\circ\text{C}$  for 5 h, and left to age for 12 h. The precipitates (Ag/HA) were filtered and washed with water and dried in an oven at  $60^\circ\text{C}$  for 12 h.

#### Design the defect and metallic Ag in $\text{Ag}_3\text{PO}_4$

The defect and metallic Ag in  $\text{Ag}_3\text{PO}_4$  were produced using co-precipitation. Typically, 0.3 g of Ag/HA was suspended in 20 mL of water and added quickly to the  $\text{AgNO}_3$  solution (1 g in 10 mL of water). The suspensions were mixed under magnetic stirring for 30 min. The yellow solids were filtered and washed with water and dried in an oven for 2 h at  $60^\circ\text{C}$ . The control sample of  $\text{Ag}_3\text{PO}_4$  was synthesized using the HA without glucose. The  $\text{Ag}_3\text{PO}_4$  as a control and the metallic Ag in  $\text{Ag}_3\text{PO}_4$  were named as SP (silver phosphate) and DMSP (defect-metallic silver in silver phosphate), respectively.

#### Photocatalytic activity

The photocatalytic activities were evaluated based on Rhodamine B (RhB) degradation under blue light irradiation [9]. A total of 0.1 g of catalyst was added to 100 mL of RhB solution (10 mg/L) in a beaker glass. The beaker was placed on the magnetic stirrer. The adsorption-desorption equilibrium was achieved at 20 min with stirring under dark conditions. After that, the blue LED lamp was turned on, and 5 mL of the sample was taken every 2 min. The sample was centrifuged at 2000 rpm for

1 h, resulting in a supernatant that was monitored by a UV-vis spectrophotometer (Shimadzu UV-1800).

The photocatalytic reaction mechanism was investigated by adding 100  $\mu\text{L}$  of scavenger (1 mol/L) to a reactor of the photocatalytic system. The scavengers of ammonium oxalate (AO), isopropyl alcohol (IPA), and benzoquinone were used to capture the hole, hydroxyl radical and superoxide radical [14]. The degradation rates of these effects were calculated by the relative percentage to the control (without scavenger).

## ■ RESULTS AND DISCUSSION

### Synthesis and Characterization

Hydroxyapatite (HA) was used as a substrate in the synthesis of  $\text{Ag}_3\text{PO}_4$ . A small amount of  $\text{Ag}_3\text{PO}_4$  on HA was created by the reaction of a small quantity of  $\text{AgNO}_3$  (0.36 mmol) with a phosphate site of HA. The reaction of HA and  $\text{AgNO}_3$  resulted in a pale-yellow suspension, suggesting the small quantity  $\text{Ag}_3\text{PO}_4$  was formed. In this step, only small phosphate of HA was reacted with  $\text{Ag}^+$

forming the  $\text{Ag}_3\text{PO}_4$ ; the large portion of HA remained and acted as support for  $\text{Ag}_3\text{PO}_4$  ( $\text{Ag}_3\text{PO}_4/\text{HA}$ ). Adding the glucose to the pale-yellow suspension changed the color into grey, indicating that all  $\text{Ag}^+$  in the crystal of  $\text{Ag}_3\text{PO}_4/\text{HA}$  was reduced into metallic Ag, forming the  $\text{Ag}/\text{HA}$ . Adding the suspended  $\text{Ag}/\text{HA}$  into the high concentration of  $\text{AgNO}_3$  solution (1 g in 10 mL of water) produced the yellow crystal of  $\text{Ag}/\text{Ag}_3\text{PO}_4$  (DMSP).

The samples of  $\text{Ag}_3\text{PO}_4$  (SP) and defect- $\text{Ag}/\text{Ag}_3\text{PO}_4$  (DMSP) showed the structure of a body-centered cubic (JCPDS No. 06-0505) [16] (Fig. 1(a)). The peak intensity of DMSP was similar to SP, indicating that the glucose did not affect the crystallinity of  $\text{Ag}_3\text{PO}_4$ . Due to small concentration, the metallic Ag cannot be detected by XRD. Fig. 1(b) shows the DRS absorption spectra of SP and DMSP. The high broad absorption of DMSP indicates that the metallic Ag prepared under glucose solution has a significant role in the absorption of  $\text{Ag}_3\text{PO}_4$  in the visible region. The metallic Ag might be incorporated on the  $\text{Ag}_3\text{PO}_4$ , forming the  $\text{Ag}/\text{Ag}_3\text{PO}_4$ .

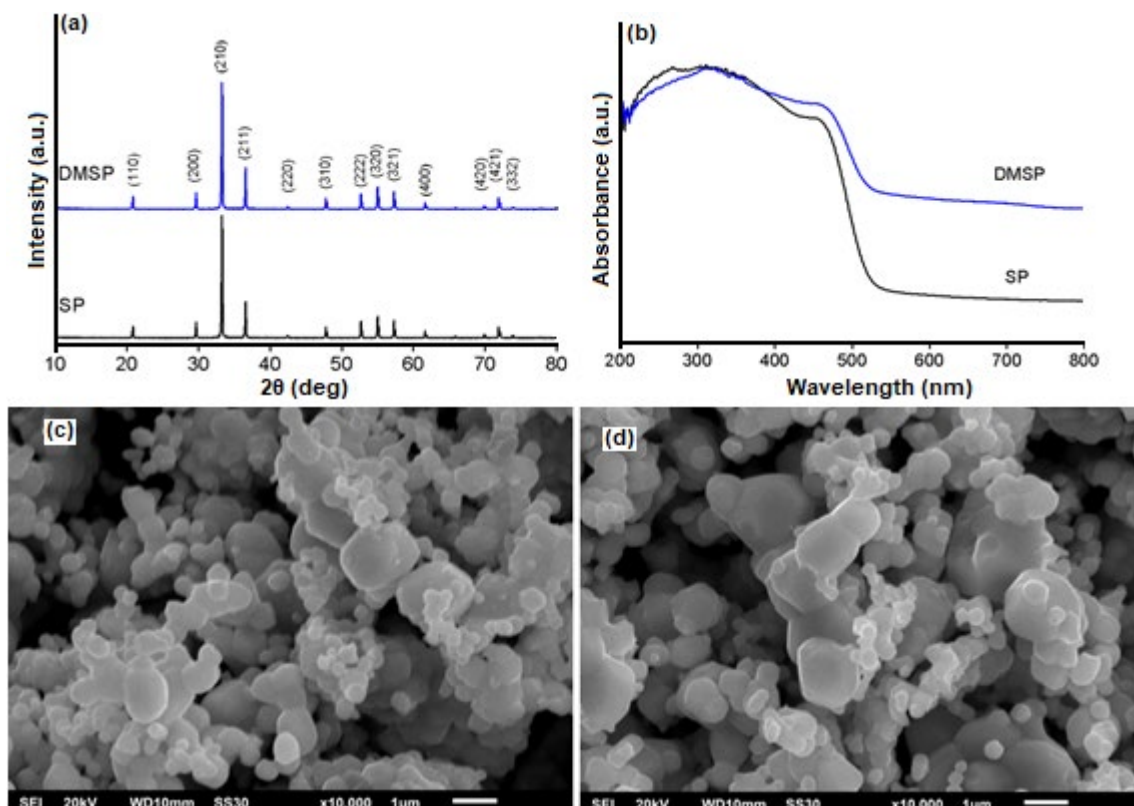


**Fig 1.** The pattern of (a) XRD, (b) DRS for the sample of SP and DMSP, and the morphology of (c) SP and (d) DMSP analyzed using SEM

The higher broad absorption in the visible region might also originate from the defect sites. It is possible that incorporating the Ag into the  $\text{Ag}_3\text{PO}_4$  generates the defect sites and produces a strong absorption in the visible region. The bandgap energy of 2.42 and 2.30 eV were calculated for SP and DMSP, respectively. The decreased bandgap energy in DMSP was suggesting that the defect might be formed.

An irregular shape was observed in both SP (Fig. 1(c)) and DMSP (Fig. 1(d)). The specific surface area of 14.3 and 15.5  $\text{m}^2/\text{g}$  is represented in SP and DMSP, respectively, and the average pore radius of SP and DMSP are 26.07 and 19.81 Å, respectively. Although the agglomeration of DMSP was high, a higher surface area is shown. It might be caused by the higher porosity of DMSP. The micropore volumes of SP and DMSP are  $8.0 \times 10^{-3}$  and  $9.5 \times 10^{-3}$   $\text{cc}/\text{g}$ , respectively. Differences in morphology, specific surface area, average pore radius, and micropore volume of the samples were not significant. Therefore, the different

catalytic activity might be highly caused by other factors, e.g., defect and metallic Ag doping.

The formation of metallic Ag was investigated using XPS. Fig. 2 shows the profile of XPS of Ag3d, P2p, and O1s for samples SP and DMSP. The broad intensities on the bottom of the Ag3d peak of DMSP were observed (Fig. 2(a)), indicating that the metallic Ag was formed. The deconvolution of XPS showed that the peak of metallic Ag with higher binding energy was clearly observed in DMSP (Fig. 2(b)). The binding energy (BE) of  $\text{Ag}3d_{5/2}$  and  $\text{Ag}3d_{3/2}$  for metallic Ag corresponded to 368.9 and 375.1 eV, respectively [17]. The FWHM of P2p in DMSP was also higher compared to the SP (Fig. 2(c)), suggesting that the metallic Ag incorporated to the  $\text{Ag}_3\text{PO}_4$  affected the bonding of phosphate ion in the lattice. Two oxygens of O-1 (530.5 eV) and O-2 (532.4 eV) in SP and DMSP were found to originate from the P–O–Ag and P=O, respectively [18].

To analyzing the defect, the atomic ratios of Ag/P,

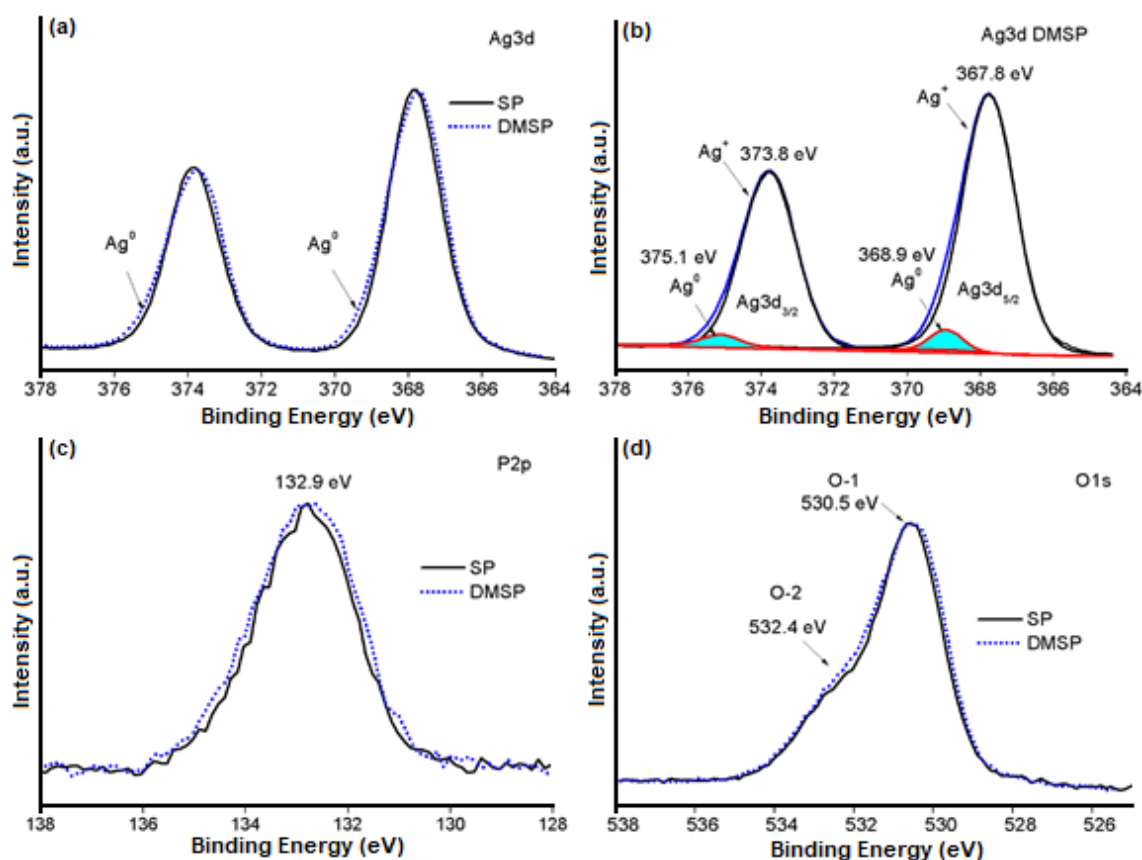


**Fig 2.** The XPS spectra of (a) Ag3d in SP and DMSP, (b) spectra deconvolution of Ag3d DMSP, (c) P2p, and (d) O1s in SP and DMSP

O/Ag, and O/P were calculated from the XPS data (Table 1). The atomic ratio of Ag/P at DMSP (2.38) was slightly higher compared to the SP (2.34), even after the sputtering treatment with Ar<sup>+</sup>. The atomic ratio of Ag/P in DMSP (2.74) stayed higher compared to the SP (2.68), indicating that the DMSP has a higher content of silver. The atomic ratio of O/Ag in DMSP is lower than that of SP, suggesting that the oxygen deficiency occurred in DMSP. Moreover, the ratio of O/P after the sputtering treatment decreased from 3.09 in SP to 3.05 in DMSP, indicating that the small quantity of oxygen had left the P–O bonding. This phenomenon ensured the formation of the oxygen vacancy in the lattice of DMSP. The formation of metallic Ag might induce the oxygen vacancy. When the Ag<sup>+</sup> is reduced to metallic Ag, the Ag<sub>3</sub>PO<sub>4</sub> becomes more negative. Based on the electro-neutrality principle [19], the anion (O<sup>2-</sup>) of Ag<sub>3</sub>PO<sub>4</sub> can now leave, resulting in oxygen vacancy.

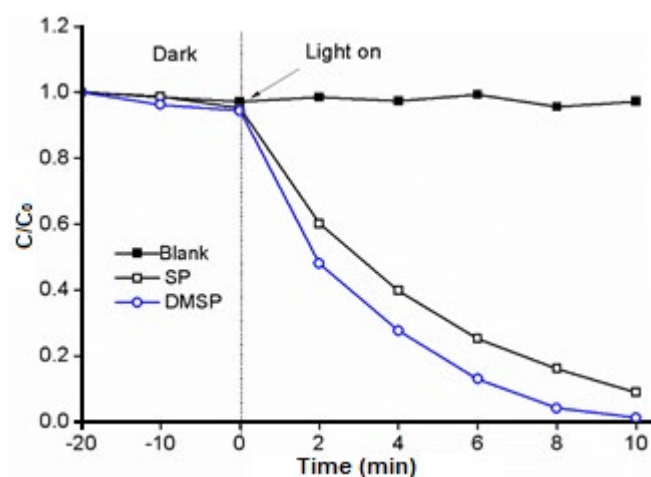
### Photocatalytic Activities

Fig. 3 displays the photocatalytic activity of SP and DMSP. The rates of photocatalytic activity were evaluated using the pseudo-first-order kinetics with the equation of  $\ln(C_0/C_t) = kt$ , where  $C_0$  and  $C_t$  are the dye concentration at time 0 and  $t$ , respectively, and  $k$  is the rate constant ( $\text{min}^{-1}$ ) [9]. When the linear of  $\ln(C_0/C_t)$  vs.  $t$  is obtained, the reaction fitted with this model. The experiment showed that all reactions followed pseudo-first-order kinetics. The rate constants of 0.23 and  $0.39 \text{ min}^{-1}$  were obtained in the sample of SP and DMSP, respectively. The photocatalytic activity of DMSP was 1.7 times higher compared to that of SP, 70% increase in rate compared to the SP.

The higher activity of DMSP was clearly caused by the metallic Ag dopant (Ag<sup>0</sup>) and oxygen vacancy. The Ag<sup>0</sup> can act as an electron acceptor for facilitating the electron transfer from Ag<sub>3</sub>PO<sub>4</sub> [18,20]. The oxygen vacancies tend to create a local state near the conduction

band (CB) in DMSP, resulting in the narrowing of the bandgap and increasing the visible absorption. When irradiated under blue light, the electrons are excited from the VB to the local state and leaves h<sup>+</sup> in the valence band (VB). This local state acts as a center for capturing the photo-generated electrons. Therefore, the recombination of photo-generated electrons and holes could be effectively suppressed, leading to an improved photocatalytic activity [18].

To understand the mechanisms of photocatalysis, the SP and DMSP were treated with the scavengers of benzoquinone (BQ), isopropanol (IPA), and ammonium oxalate (AO) to trap the species of •O<sub>2</sub><sup>-</sup>, •OH, and h<sup>+</sup>, respectively [14]. The results are shown in Fig. 4. The rate constants of SP were measured and found to be 0.234, 0.161, 0.088,  $0.033 \text{ min}^{-1}$  for samples without scavenger, IPA, BQ, and AO, respectively. Based on these results, the relative percentage of 68.8, 37.7, and 14.0% are found in IPA, BQ, and AO, respectively. The rate constants of DMSP were also measured, resulting in 0.353, 0.259, 0.106,



**Fig 3.** The photocatalytic activity of SP and DMSP evaluated using the degradation of Rhodamine B (RhB) with an initial concentration of 10 mg/L and a volume of 100 mL

**Table 1.** The atomic ratio of Ag/P, O/Ag and O/P in Ag<sub>3</sub>PO<sub>4</sub> and Ag/Ag<sub>3</sub>PO<sub>4</sub> measured using XPS

Samples	Before sputtering			After sputtering		
	Ag/P	O/Ag	O/P	Ag/P	O/Ag	O/P
SP	2.34	1.65	3.86	2.68	1.15	3.09
DMSP	2.38	1.63	3.89	2.74	1.11	3.05

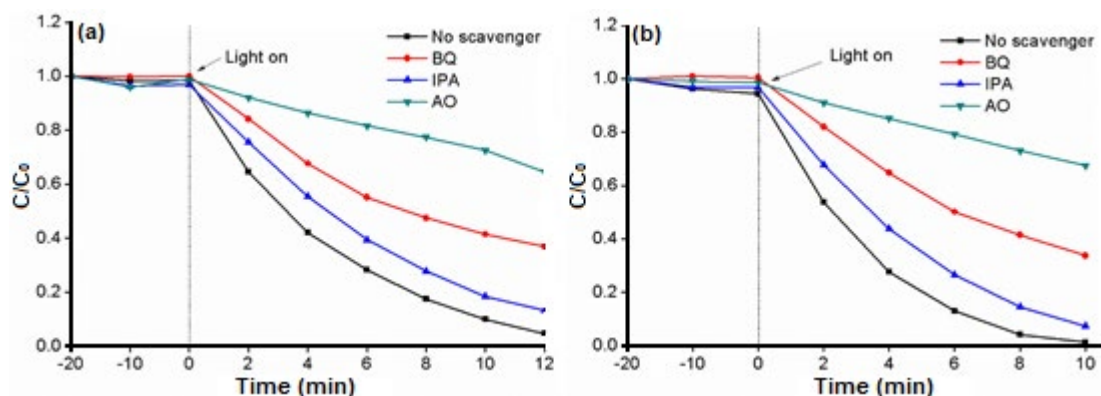


**Fig 4.** The evaluation of the photocatalytic mechanism in SP(a) and DMSP(b) using the scavengers (BQ: benzoquinone, IPA: isopropyl alcohol, and AO: ammonium oxalate)

0.039  $\text{min}^{-1}$  for the sample without scavenger, IPA, BQ, and AO, respectively, and the relative percentage of 73.4, 30.1, and 11.1% were also calculated for IPA, BQ, and AO, respectively. The data showed that the photocatalytic reactions in DMSP were more suppressed due to BQ and AO, indicating that the role of  $\bullet\text{O}_2^-$  and  $\text{h}^+$  being higher in the mechanism.

## CONCLUSION

The defect and metallic Ag in  $\text{Ag}_3\text{PO}_4$  photocatalyst can be created using hydroxyapatite and glucose using the co-precipitation method. This preparation could decrease the ratio of O/Ag and create a small metallic Ag that generates the oxygen vacancy and doping in the photocatalyst, respectively. The phenomena resulted in an increased photocatalytic activity under blue light irradiation.

## ACKNOWLEDGMENTS

This research was partly financially supported by the Directorate of Research and Community Service, Deputy of Strengthening Research and Development, Ministry of Research and Technology/National Research and Innovation Agency, Number: 176/SP2H/ADM/LT/DRPM/2020.

## REFERENCES

- [1] Sofi, F.A., Majid, K., and Mehraj, O., 2018, The visible light driven copper based metal-organic-framework heterojunction:HKUST-1@Ag- $\text{Ag}_3\text{PO}_4$  for plasmon enhanced visible light photocatalysis, *J. Alloys Compd.*, 737, 798–808.
- [2] Mohanty, S., Babu, P., Parida, K., and Naik, B., 2019, Surface-plasmon-resonance-induced photocatalysis by core-shell  $\text{SiO}_2@\text{AgNCs}@\text{Ag}_3\text{PO}_4$  toward water-splitting and phenol oxidation reactions, *Inorg. Chem.*, 58 (15), 9643–9654.
- [3] Ma, F., Yang, Q., Wang, Z., Liu, Y., Xin, J., Zhang, J., Hao, Y., and Li, L., 2018, Enhanced visible-light photocatalytic activity and photostability of  $\text{Ag}_3\text{PO}_4/\text{Bi}_2\text{WO}_6$  heterostructures toward organic pollutant degradation and plasmonic Z-scheme mechanism, *RSC Adv.*, 8 (28), 15853–15862.
- [4] Kim, Y.G., and Jo, W.K., 2019, Efficient decontamination of textile industry wastewater using a photochemically stable  $n-n$  type  $\text{CdSe}/\text{Ag}_3\text{PO}_4$  heterostructured nanohybrid containing metallic Ag as a mediator, *J. Hazard. Mater.*, 361, 64–72.
- [5] Shen, Y., Zhu, Z., Wang, X., Khan, A., Gong, J., and Zhang, Y., 2018, Synthesis of Z-scheme  $\text{g-C}_3\text{N}_4/\text{Ag}/\text{Ag}_3\text{PO}_4$  composite for enhanced photocatalytic degradation of phenol and selective oxidation of gaseous isopropanol, *Mater. Res. Bull.*, 107, 407–415.
- [6] Liu, Y., Fang, L., Lu, H., Li, Y., Hu, C., and Yu, H., 2012, One-pot pyridine-assisted synthesis of visible-light-driven photocatalyst  $\text{Ag}/\text{Ag}_3\text{PO}_4$ , *Appl. Catal., B*, 115-116, 245–252.

- [7] Bi, Y., Hu, H., Ouyang, S., Jiao, Z., Lu, G., and Ye, J., 2012, Selective growth of metallic Ag nanocrystals on  $\text{Ag}_3\text{PO}_4$  submicro-cubes for photocatalytic applications, *Chem. Eur. J.*, 18 (45), 14272–14275.
- [8] Gondal, M.A., Chang, X., Sha, W.E.I., Yamani, Z.H., and Zhou, Q., 2013, Enhanced photoactivity on Ag/ $\text{Ag}_3\text{PO}_4$  composites by plasmonic effect, *J. Colloid Interface Sci.*, 392, 325–330.
- [9] Sulaeman, U., Hermawan, D., Andreas, R., Abdullah, A.Z., and Yin, S., 2018, Native defects in silver orthophosphate and their effects on photocatalytic activity under visible light irradiation, *Appl. Surf. Sci.*, 428, 1029–1035.
- [10] Zhai, H., Yan, T., Wang, P., Yu, Y., Li, W., You, J., and Huang, B., 2016, Effect of chemical etching by ammonia solution on the microstructure and photocatalytic activity of  $\text{Ag}_3\text{PO}_4$  photocatalyst, *Appl. Catal., A*, 528, 104–112.
- [11] Xie, Y.P., and Wang, G.S., 2014, Visible light responsive porous Lanthanum-doped  $\text{Ag}_3\text{PO}_4$  photocatalyst with high photocatalytic water oxidation activity, *J. Colloid Interface Sci.*, 430, 1–5.
- [12] Chong, R., Cheng, X., Wang, B., Li, D., Chang, Z., and Zhang, L., 2016, Enhanced photocatalytic activity of  $\text{Ag}_3\text{PO}_4$  for oxygen evolution and methylene blue degeneration: Effect of calcination temperature, *Int. J. Hydrogen Energy*, 41 (4), 2575–2582.
- [13] Cruz-Filho, J.F., Costa, T.M.S., Lima, M.S., Silva, L.J., Santos, R.S., Cavalcante, L.S., Longo, E., and Luz Jr., G.E., 2019, Effect of different synthesis methods on the morphology, optical behavior, and superior photocatalytic performances of  $\text{Ag}_3\text{PO}_4$  submicrocrystals using white light-emitting diodes, *J. Photochem. Photobiol., A*, 377, 14–25.
- [14] Sulaeman, U., Suhendar, S., Diastuti, H., Riapanitra, A., and Yin, S., 2018, Design of  $\text{Ag}_3\text{PO}_4$  for highly enhanced photocatalyst using hydroxyapatite as a source of phosphate ion, *Solid State Sci.*, 86, 1–5.
- [15] Wang, J.D., Liu, J.K., Lu, Y., Hong, D.J., and Yang, X.H., 2014, Catalytic performance of gold nanoparticles using different crystallinity HAP as carrier materials, *Mater. Res. Bull.*, 55, 190–197.
- [16] Cui, X., Tian, L., Xian, X., Tang, H., and Yang, X., 2018, Solar photocatalytic water oxidation over  $\text{Ag}_3\text{PO}_4/\text{g-C}_3\text{N}_4$  composite materials mediated by metallic Ag and graphene, *Appl. Surf. Sci.*, 430, 108–115.
- [17] Zhang, J., Yu, K., Yu, Y., Lou, L.L., Yang, Z., Yang, J., and Liu, S., 2014, Highly effective and stable  $\text{Ag}_3\text{PO}_4/\text{WO}_3$  photocatalysts for visible light degradation of organic dyes, *J. Mol. Catal. A: Chem.*, 391, 12–18.
- [18] Dong, P., Hou, G., Liu, C., Zhang, X., Tian, H., Xu, F., Xi, X., and Shao, R., 2016, Origin of activity and stability enhancement for  $\text{Ag}_3\text{PO}_4$  photocatalyst after calcination, *Materials*, 9 (12), 968.
- [19] Du, X., Ma, G., and Zhang, X., 2019, Oxygen vacancy-confined  $\text{CoMoO}_4@/\text{CoNiO}_2$  nanorod arrays for oxygen evolution with improved performance, *Dalton Trans.*, 48 (27), 10116–10121.
- [20] Bi, Y., Hu, H., Ouyang, S., Jiao, Z., Lu, G., and Ye, J., 2012, Selective growth of  $\text{Ag}_3\text{PO}_4$  submicro-cubes on Ag nanowires to fabricate necklace-like heterostructures for photocatalytic applications, *J. Mater. Chem.*, 22 (30), 14847–14850.